Biotechnology Journal

www.biotechnology-journal.com

High Cell Density Perfusion Culture has a Maintained Exoproteome and Metabolome

*Leila Zamani, Magnus Lundqvist, Ye Zhang, Magnus Aberg, Fredrik Edfors, Gholamreza Bidkhori, Anna Lindahl, Axel Mie, Adil Mardinoglu, Raymond Field, Richard Turner, Johan Rockberg, and Veronique Chotteau**

The optimization of bioprocesses for biopharmaceutical manufacturing by Chinese hamster ovary (CHO) cells can be a challenging endeavor and, today, heavily relies on empirical methods treating the bioreactor process and the cells as black boxes. Multi-omics approaches have the potential to reveal otherwise unknown characteristics of these systems and identify culture parameters to more rationally optimize the cultivation process. Here, the authors have applied both metabolomic and proteomic profiling to a perfusion process, using CHO cells for antibody production, to explore how cell biology and reactor environment change as the cell density reaches $\geq 200 \times 10^6$ cells mL^{-1}. The extracellular metabolic composition obtained in perfusion mode shows a markedly more stable profile in comparison to fed-batch, despite a far larger range of viable cell densities in perfusion. This stable profile is confirmed in the extracellular proteosome. Furthermore, the proteomics data shows an increase of structural proteins as cell density increases, which could be due to a higher shear stress and explain the decrease in cell diameter at very high cell densities. Both proteomic and metabolic results shows signs of oxidative stress and changes in glutathione metabolism at very high cell densities. The authors suggest the methodology presented herein to be a powerful tool for optimizing processes of recombinant protein production.

1. Introduction

Mammalian cell lines have become increasingly important for the production of recombinant therapeutic glycoproteins in fed-batch or perfusion modes. A detailed understanding of the factors that contribute to the productivity and variability of cell cultures is important for the control and optimization of manufacturing processes. In contrast to fed-batch mode, in perfusion mode, the spent medium is continuously removed while fresh medium is added.[1–4] This can prolong the healthy culture length and reduce the residence time of the product of interest in the bioreactor, a crucial factor for unstable glycoproteins. Perfusion is used for biopharmaceutical production to generate high cell density seeds for production bioreactors, for cell bank manufacturing or for the production of proteins as research tools. An attractive feature of this mode is the possibility to achieve very high cell densities,[5,6] enabling intensified processes in bioreactor

Dr. L. Zamani, Dr. Y. Zhang, Dr. V. Chotteau
Department Industrial Biotechnology
School of Engineering Sciences in Chemistry, Biotechnology, and Health
KTH-Royal Institute of Technology
106 91 Stockholm, Sweden
E-mail: veronique.chotteau@biotech.kth.se

Dr. M. Lundqvist, Dr. Y. Zhang, Dr. J. Rockberg, Dr. V. Chotteau
School of Engineering Sciences in Chemistry, Biotechnology, and Health
Wallenberg Centre for Protein Research
KTH-Royal Institute of Technology
10691 Stockholm, Sweden

Dr. M. Lundqvist, Dr. J. Rockberg, Dr. V. Chotteau
School of Engineering Sciences in Chemistry, Biotechnology, and Health
AdBIOPRO, Centre for Advanced Bioproduction by Continuous Processing
KTH-Royal Institute of Technology
106 91 Stockholm, Sweden

DOI: 10.1002/biot.201800036

Dr. M. Aberg
Department of Analytical Chemistry
Stockholm University
106 91 Stockholm, Sweden

Dr. F. Edfors, Dr. G. Bidkhori, Dr. A. Mardinoglu
School of Engineering Sciences in Chemistry, Biotechnology, and Health
Science for Life Laboratory
KTH-Royal Institute of Technology
171 65 Stockholm, Sweden

Dr. A. Lindahl
Department of Oncology-Pathology
Science for Life Laboratory
Karolinska Institutet
171 65 Solna, Sweden

Dr. A. Mie
Department of Clinical Science and Education
Karolinska Institute
118 83 Solna, Sweden

Dr. R. Field, Dr. R. Turner
Biopharmaceutical Development
MedImmune
CB21 6GH Cambridge, United Kingdom

volumes that are much smaller than fed-batch mode for an equivalent production. The main advantages are reductions of capital expenditure costs, footprint and operation scale, as well as suitability with disposable equipment and associated advantage of flexibility and transferability. The environment within the reactor in fed-batch processes is significantly more variable than in perfusion processes due to the progressive accumulation of by-products and the gradual depletion of nutrients, causing changes in the cellular metabolism. In contrast, perfusion provides a more constant environment, which promotes cellular health, as demonstrated for key components such as glucose and the amino acids.[7,8]

In the past decade, there has been progress in analytical technologies and data mining, enabling metabolite profiling of recombinant protein production. Several studies were carried out with CHO cells cultures to understand and model the cell metabolism in batch and fed-batch modes[9–18] while a very limited amount of these studies have been performed for cultures in perfusion mode. Goudar et al.[19] published an analysis of the metabolic fluxes in CHO cells perfusion culture using ^{13}C glucose NMR, showing very stable uptake rates of most of the studied nutrients. The metabolomic profile of Baby Hamster Kidney cell perfusion cultures used for manufacturing was characterized in[20] and,[21] showing consistency throughout the culture and the scales (e.g., small- vs. commercial scale), but variations associated to the cell age studied in 150 days long cultures. Due to the wide range in molecule size and complexity, the study of a complete metabolome is highly challenging by a single analytical method. Liquid chromatography-mass spectrometry (LC/MS) can detect a wide range of metabolites and is widely used.[22–25] The extraction of relevant information from the huge data sets generated by such approaches is highly challenging due to the complexity of several factors: the biological samples, the interactions between the variables, the variability of the signals, and can be performed by on several multivariate data analysis techniques,[23,26,27] e.g., Principal component analysis (PCA),[23,28] Partial Least Square (PLS) regression,[29] and Partial Least Squares-discriminant analysis (PLS-DA).[23]

A comprehensive description of the protein composition can also reveal biological circumstances that hopefully will provide guidance for host strain and process development. Several aspects of CHO cells in recombinant protein production have formerly been investigated by means of proteomic methodologies. For instance, supernatant differences between transfected and non-transfected clones,[30] influence of relatively small variations of protein sequence and their effect on specific productivity,[31] and culture conditions in fed-batch mode[32] are a few examples of such investigations.

In the present study, the extracellular metabolic profiles obtained in perfusion mode was first compared to fed-batch operation by LC/MS with full scan acquisition. Complementarily to the metabolomics data, the exoproteome variation of the perfusion reactor as the cell density of the bioreactor increased from low to extremely high levels, was studied using label-free shotgun LC-MS. The metabolites and proteins that prominently changed throughout the experiment, as the cell density reached an extraordinary level of 200 millions viable cells per milliliter (MVC/mL), were then identified and discussed.

2. Experimental Section

2.1. Chemicals

Acetonitrile (ACN) and sodium hydroxide were purchased from MERCK (Darmstadt, Germany). Formic acid (FA) was purchased from Fluka (Buchs, Switzerland). Milli-Q quality water was used in all experiments.

2.2. CHO Cell Cultivations

An IgG1-producing research cell line DHFR- CHO was used in a perfusion culture (TFF#10) and two fed-batch runs (FB#111, FB#16) performed in a wave bioreactor as described elsewhere,[5,6] and using IS CHO CD XP medium supplemented with IS-CHO Feed-CD XP (all Irvine Scientific) in perfusion mode or IS CHO CD XP medium supplemented with feed medium Efficient Feed A/B (Invitrogen) in fed-batch mode. A TFF cell separation device (ReadyToProcess filter-GE Healthcare) was used to operate a perfusion rate of 1 to 10 reactor volumes/day using a cell specific perfusion rate (CSPR). The set points were 35% dissolved oxygen concentration, pH 7.0, 37 °C and working volume 4 L, except that in the fed-batch runs the working volume was 2 L at inoculation and that the temperature was shifted to 35.5 °C at days 7-end in FB#16.

2.3. Bioreactor Culture Daily Analyses

Culture medium samples were daily collected from the reactor, and the following parameters were measured using a Bioprofile FLEX system (Nova Biomedical): cell density, viability, average cell diameter (ACD), pH, partial pressure of CO_2 (pCO_2) and the concentrations of glucose, lactate, glutamine, and ammonia. The antibody (MAb) concentration was measured by protein A HPLC. Cell specific rates of glucose (q_{glc}) and glutamine (q_{gln}) consumptions and of lactate (q_{lac}), ammonium (q_{amm}), and MAb (q_{MAb}) productions were calculated according to.[5,6] After sampling, cell-free samples obtained by centrifugation were stored at −80 °C.

2.4. Centrifugal Filtering

Samples were prepared using pre-rinsed Microcon centrifugal filter devices (cellulose membranes, 10 kDa molecular weight cut-off, Millipore, Bedford, USA). The filter reservoirs were then washed with 300 µl of 0.1 M NaOH, and then repeatedly washed with 300 µl volumes of deionized water to remove residual basicity. The sample reservoir was then placed in a new tube and 90 µl of a sample was applied. The resulting assembly was centrifuged at 13 000 g for 15 min. The eluate containing the low molecular weight material was then transferred to sample vials and stored at −20 °C. Triplicates of all samples were prepared and analyzed to evaluate the repeatability of the method. Blank (MQ) samples were also prepared and filtered in triplicate. In addition, quality control (QC) samples were prepared by pooling prepared samples collected on different days. The resulting

mixed prepared samples were aliquoted into vials and stored at −20 °C.

2.5. UHPLC/ESI-MS

The extracted <10 kDa fractions were analyzed using an ultra-high-pressure LC (UHPLC) system (Agilent 1290) with an Ascentis® Express C18 column (2.1 × 150 mm, 2.7 μm) (Supelco Analytical, PA, USA) together with a guard column (2.1 × 15 mm, 2,7 μm) (Supelco Analytical), at a temperature of 37 °C, with mobile phase of variable proportions of H2O:FA (1,000:1, v/v; solution A) and ACN:FA (1,000:1, v/v, solution B). Elution was initially performed at a flow rate of 0.4 mL min^{-1} with 5% B for 1 min. The content of B in the eluent was then increased linearly to 40% over 6 min, followed by a linear increase to 100% B over 2 min and an isocratic wash with 100% B that lasted for an additional 2 min. The column was then equilibrated for the next injection by washing with 100% A for 1.5 min. The total time required for a single analytical run (including washing and equilibration) was 13 min. The temperature of the auto-injector was 4 °C, and the injection volume was 5 μl. The compounds eluting from the analytical column were detected using an ESI-QTOF MS instrument (Agilent 6540 Accurate Mass Q-TOF) with Agilent Jet Stream Technology in both positive and negative ion modes (in different injections). The instrument was calibrated in the high-resolution (4 GHz, High Res Mode), lower mass range ($m z^{-1} < 1700$) in both ionization modes. Centroid data were acquired at a rate of 15.92 spectra/s rate using a Mass Hunter workstation (Agilent) within a mass range of 100–1700 $m z^{-1}$ and with a time window of 10. The drying gas temperature was set at 300 °C, the drying gas flow at 8 L min^{-1}, the nebulizer pressure at 35 psi, the capillary voltage (Vcap) at 3500 V, and the fragmentor voltage at 100 V. In the targeted MS/MS experiments, the collision energy was set at 20 V and the product ion scan range was 50–1000 Da. A retention time window of ±0.2 min and a medium (m/z 4) precursor ion isolation width was used with a scan rate of 9.5 spectra/s. High-purity nitrogen was introduced into the collision cell as the fragmentation gas. Reference masses of m/z 121.0508 and 922.0098 in positive ionization mode and m/z 112.9856 in negative ionization mode were continuously introduced into the ionization chamber to maintain accurate mass calibration. To ensure a constant quality of the analytical method during the batch analysis, and the validity of the acquired data, pooled QC samples were analyzed every 10 samples, all the samples were prepared and analyzed in triplicate in randomized order, and blank samples (where no sample was injected) were run every 8–10 experimental samples. The QC samples clustered together on the unsupervised PCA scores plots, as did triplicate samples taken on the same day from the same run, indicating that the analytical process and data pre-processing techniques used were reliable and of good quality. Several biomarkers were identified by obtaining accurate mass data for the corresponding peaks and by further MS/MS analysis of their [M+H]+ or [M-H]- adducts. The metabolite identities were subsequently confirmed by comparing their MS2 fragmentation patterns in positive and negative mode (in cases where the metabolite was detected in both spectra) to entries in metabolite databases Metlin and the human metabolite database (HMDB). Isotope patterns were also used to confirm metabolite identities where applicable.

2.6. Data and Data Processing

Each compound gave rise to many detected peaks, including adducts, isotopologues, and fragments. Prior statistical analyses, the data for the different samples collected during individual experiments were synchronized by peak detection and alignment, to correct for shifts in retention time and, to a lesser extent, in m/z values, due to potential peak shifts (from instrumental drift, variations in the separation chemistry and varying sample properties[33]). Line spectra were exported as files in mzData format and examined using TracMass[34] at Stockholm University. Peak detection and alignment were performed as described by Tengstrand et al.[35] Approximately 10 000 peaks with intensities above 1000 were detected in each sample. For each experiment, a matrix was generated that included the retention time, m/z and intensity of each detected ion. The metabolomics multivariate statistical analyses were performed using Unscrambler-X (CAMO, Norway). Peaks found in all samples and in all three replicates of at least one sample were selected for more detailed multivariate analysis. All data were auto-scaled and area normalized before multivariate analyses. PCA was used to visualize the complex data set and identify similarities and differences between samples. PLS was used to identify relationships between the LC-MS data and parameters of the cell cultures, i.e., viable cell density, q_{glc}, q_{gln}, q_{lac}, q_{amm}, and q_{MAb}, temperature. Data from both positive and negative ion spectra were pooled and analyzed together.

2.7. Proteomics

Supernatant samples from seventeen days (3, 5, 10, 12, 14, 18, 22, 23, 26, 27, 28, 30, 38, 39, 40, 41, and 45) were prepared for LC-MS/MS analysis by the filter-aided sample preparation (FASP) method[36] using a 10 kDa cut-off filter (PALL). Samples were diluted 1:2 in 8 M Urea and applied to the filter for washing, reduction and alkylation as described in the original protocol.[36] After overnight digestion with porcine trypsin (Sigma) in a 1:50 E:S (w/w) ratio, peptides were extracted and desalted using in-house prepared StageTips packed with Empore C18 Bonded Silica matrix (3M, Saint Paul, MN).[37] Three layers of octadecyl membrane were placed in 200-μl pipette tips and the membrane was activated by addition of 100% ACN and centrifugation at 2000 rcf for 1 min. Equilibration of membrane was done by supplying 0.1% FA, MQ and centrifugation at 2000 rcf for 1 min. The samples were acidified with 7 μl 10% FA before addition onto the membrane, followed by centrifugation at 2000 rcf for 1 min. The membrane was washed twice with 0.1% FA, MQ before the peptides were eluted in two steps using 60% ACN, MQ. Desalted peptides were analyzed by BCA and subsequently vacuum-dried and stored at −20 °C before LC-MS/MS analysis.

An UltiMate 3000 binary RS nano system (Thermo Scientific) with an EASY-Spray ion source was used for liquid chromatography. The samples were stored in their lyophilized state and resuspended by the autosampler before injection as 1 μg

peptides were loaded onto column. Three technical replicates were used for each sample and material was loaded onto an Acclaim PepMap 100 trap column (75 μm × 2 cm, C18, 3 μm, 100 Å) and washed 5 min at 0.250 μl min^{-1} with solvent A (95% H2O, 5% DMSO, 0.1% FA), and subsequently separated on a PepMap 800 C18 column (15 cm × 75 μm, 3 μm). The gradient changed from solvent A to solvent B (90% ACN, 5% H2O, 5% DMSO, 0.1% FA) at a constant flow of 0.250 μl min^{-1}, to 43% solvent B for 40 min, and was then increased up to 55% during 10 min and was followed by a steep increase to 100% B for 2 min. Online LC–MS/MS was done using a Q-Exactive HF mass spectrometer (Thermo Scientific). A Top5 MS-method with master scans was carried out at 60 000 resolution (mass range 300–1,600 m z^{-1}, AGC 3e6) before five consecutive MS/MS events at 30 000 resolution (AGC 1e5, underfill ratio 0.1%) with normalized collision energy of 25. The mass spectrometry proteomics data have been deposited to the ProteomeXchange Consortium via the PRIDE[38] partner repository with the dataset identifier PXD008760.

Raw files were searched with MaxQuant[39] (version 1.5.7.4) using the standard settings, and the Andromeda search engine using the *Cricetulus griseus* reference proteome (Uniprot-ID: #UP000001075, downloaded in January 2017) together with Immunoglobulin heavy constant gamma 1 (sp|P01857|IGHG1_HUMAN). The iBAQ values for the technical replicates were combined and normalized by removing contaminants and reverse hits and the remaining values were divided by the total iBAQ intensity for their corresponding day.

Pearson correlations of the sample distribution were calculated with proteins without missing values (950 in total). Spearman correlations were used to determine correlations between proteins, cell density and pCO_2. Proteins without missing values were used. Changes in abundance for individual proteins between cell density groups were calculated by Welch's *t*-test and a doubling or halving in intensity together with an adjusted *p*-value (FDR) below 0.05 was considered a significant change. Comparisons were skipped if less than three non-missing values were encountered for any group.

3. Results

3.1. Experimental Overview

The main goal of this article is to present how the metabolic and proteomic landscape evolve during a perfusion run as the cell density increases from low to extremely high levels. The effect of the cell density on the reactor process and its main parameters has previously been described.[5,6] A brief summary of selected meta-observations is given here to set the stage for the omics analyses.

A bioreactor perfusion culture (run TFF#10) was performed for more than 40 days with medium renewal rate proportional to the cell density, i.e., cell specific perfusion rate (**Figure 1**). The cell density was first increased to 30 MVC mL^{-1}, then maintained at 20–30 MVC mL^{-1} by cell bleed, and allowed for growth up to 80 MVC mL^{-1}. After this, it was maintained by bleeds at 85-100 and 120–130 MVC mL^{-1}, and followed by a last growth phase up to 214 MVC mL^{-1}. At this latter density, limitations occurred due to the suspension's viscosity and the very short inter-cellular distances jeopardizing the filtration.[5] The main cell specific parameters (i.e., ACD, q_{glc}, q_{gln}, q_{lac}, q_{amm}) did not markedly vary at cell densities between 10 and 160 MVC mL^{-1}. Above this range, both q_{gln} and ACD decreased, although the other cell specific parameters were unaffected. q_{MAb} did not markedly change at cell densities between 10 and 130 MVC mL^{-1} but decreased above this range. Finally, the pCO_2 in the culture increased with the cell density.

3.2. High Viable Cell Density Perfusion Metabolomics

Of the 33 samples representatives of the different stages given in Section 3.1, 29 samples were included in the metabolomics data set, and four samples were excluded as outliers: two replicates from days 5 and 44 were outliers due to failure in sample preparation, and two other replicates from day 5 were outliers because they did not fall within the boundaries of a 2D tolerance ellipse plot.[40] The PCA score plot (**Figure 2**A) showed data spreading between −0.004 and 0.005 at most according to PC1 and PC2 with no highly systematic trend as function of time. The metabolomic profile in perfusion mode was then compared to 20 supernatant samples of consecutive days from two fed-batch runs, FB#11 run performed at 37 °C and FB#16 run initially at 37 °C then reduced to 35.5 °C from day 7 onwards, in a PCA score plot (Figure 2B). The fed-batch samples mostly varied in PC1 while perfusion samples were mostly defined by PC2. Despite the wide range of cell densities, the perfusion samples were significantly closer to each other than the fed-batch samples (Figure 2A). Contrary to the perfusion samples, in fed-batch the samples were distributed in a consistent pattern over time. These observations indicate that the extracellular metabolite profile in perfusion mode was significantly more stable than in fed-batch, despite the much larger range of cell densities and longer cultivation period used in this run. Similar observations were previously reported based on measurements of the concentrations of glucose, lactate, and amino acid.[1–4,19] The spent medium composition remained rather unchanged due to the bioreactor medium renewal at a rate proportional to the cell density.[5]

A PLS regression model was generated to study the correlations between the LC/MS exometabolome data (X-values) of the TFF#10 perfusion run and the measured bioreactor parameters (Y-values) such as the viable cell density, the cell specific rates of consumption/production of the main metabolites, and the ACD for days 8–45. Table S1, Supporting Information, shows the results of this modelling exercise for different Y-values that were validated by cross-validation. There was a strong correlation between the composition of the exometabolome and the cell density between days 8 and 45, at cell densities 10–214 MVC mL^{-1}. No correlations between the exometabolome and q_{lac}, q_{amm}, or q_{MAb} were identified, while q_{gln} and ACD, as well as q_{glc} to some extent, were correlated with the composition of the exometabolome only between days 38 and 45, when the viable cell density was ≥127 MVC mL^{-1}. These results show that the metabolism of the cells changed at densities higher than 127 MVC mL^{-1}. We have previously observed that the cellular metabolism in perfusion mode did

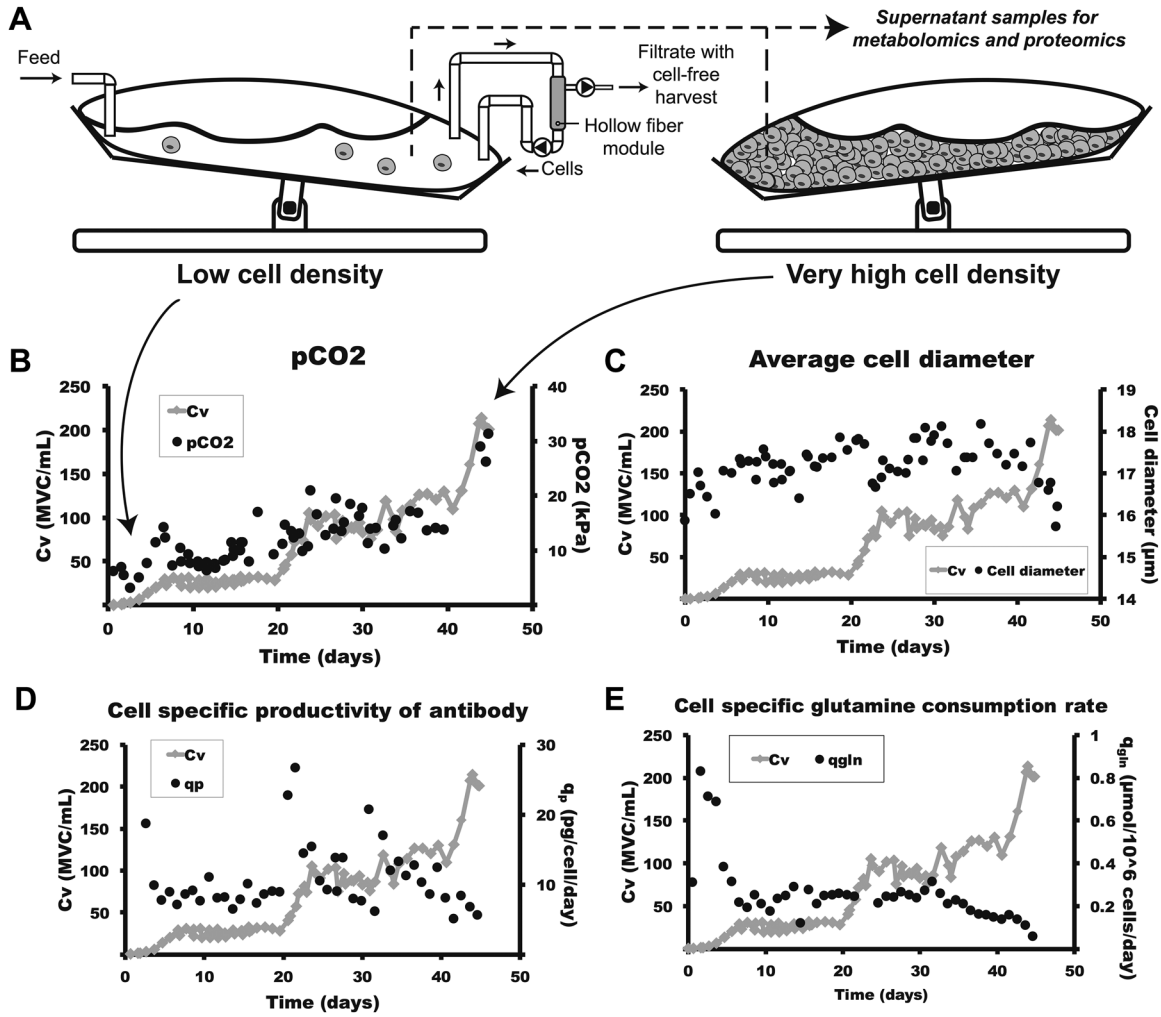

Figure 1. Experimental setup and basic bioprocess parameters. A) Scheme of the perfusion culture system. B–E) Examples of process parameters (black circle) with cell growth profiles (gray diamond).

not markedly change with the cell density $\leq$160 MVC mL^{-1} and that q_{gln} and ACD varied above this threshold.[5] The exometabolome thus confirmed and refined these previous observations.

3.3. High Viable Cell Density Perfusion Proteomics

As the cell density of the perfusion culture expanded from low to exceptionally high levels (3.3–201 MVC mL^{-1}), 17 supernatant samples were analyzed by label-free shotgun proteomics to explore the variation in proteome. A sample distance matrix of the replicates based on Pearson correlations and proteins without missing values, overall demonstrated high similarities between the samples with most correlation coefficients well above 0.9 (**Figure 3**A). Two replicates for both day 39 and 40 were excluded as they were considered outliers. The samples clustered in four groups: days 3, 5, and 10 with medium cell density between 3.32 and 30 MVC mL^{-1}; days 12, 14, 18, 22, 23, and 30 with high cell density between 30 and 82 MVC mL^{-1}; days 26, 27, 28, 30, 38, and 41 with very high cell density between 94 and 126 MVC mL^{-1}; day 45 with extreme cell density 201 MVC mL^{-1}. Notice that although the density of 30 MVC mL^{-1} at day 10 had been established at stable level for 70 h, day 10's sample clustered better with anterior days than posterior days, which indicates that the establishment of a steady state required a longer time than 70 h. The proteins of the "medium," "high," and "very high" cell densities were compared using Welsh's *t*-test to determine the most prominent differences between these groups (Figure 3B–D). See Supporting Information S2 for all proteins with significant changes. Days 39 and 40 were excluded as two thirds of the technical replicates were considered outliers and the extreme group was not examined, as the statistical relevance of one biological sample was considered too low. To be regarded as significant change, a doubling or halving in intensity, as well as an adjusted *p*-value below 0.05 was required. With this threshold, no significant changes were observed between "medium" and "high," while "high" vs. "very high" revealed 51 significant changes and "medium" vs. "very high" 83 proteins, representing respectively 2.9% and 7.2% of the

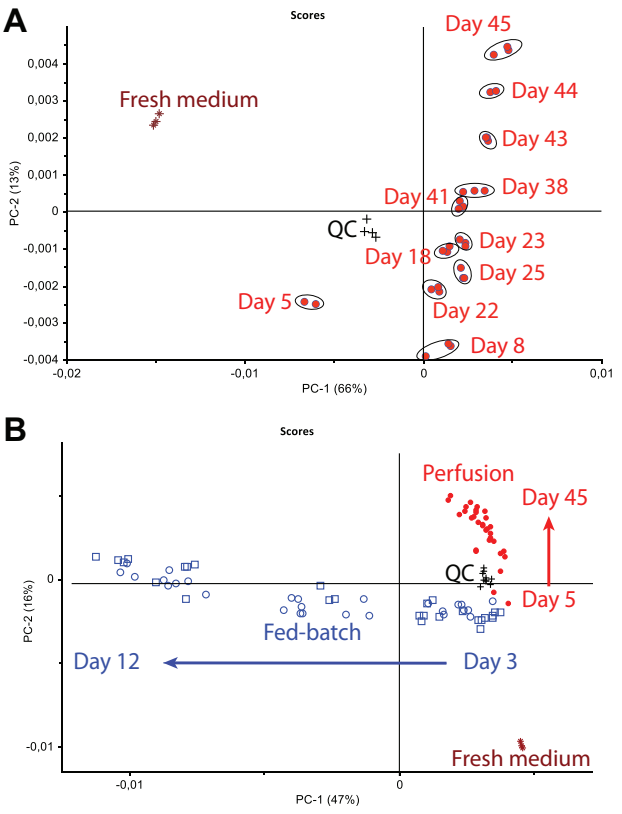

Figure 2. PCA score plots of the exometabolomics. A) Replicate samples (indicated by encirclement) taken at different days in perfusion culture TFF#10 (red filled circles), fresh medium samples (asterisk) and QC samples (plus). Data spread between −0.004 and 0.005 at most according to PC1 and PC2 with no systematic trend as function of time. B) Samples taken at different days in perfusion culture TFF#10 (red filled circles) and in fed-batch FB#11 (open blue circles) and FB#16 (squares), fresh medium samples (asterisk) and QC samples (plus). In A and B, the models were calibrated by all the data of the score, i.e., from the culture run(s), the fresh medium and QCs. The data in both fed-batch runs spread mostly along PC1 between −0.011 and 0.004 with a systematic trend as function of time from day 3 to day 12, while the data in the perfusion run were much more clustered, spreading mostly along PC2 between −0.00007 and 0.003, despite the much larger range of cell densities and the longer culture (between day 5 and day 45).

compared proteins. In total, close to 2500 proteins were identified, and most of the samples had close to 2000 identified proteins without missing values, see Figure 3E. The heavy chain of the antibody was included in the MaxQuant search and it corresponded to 35% of total iBAQ intensity for the first two samples and was later stable around 15% of the total iBAQ intensity. The drop in relative abundance of antibody can be explained by the fact that fewer proteins were detected in the first two samples. Additionally, after this time point (day 5), the intracellular leakage was bigger as proteins predicted to be intracellular accounted for around 70% of the total iBAQ compared to 45% for the first two samples (see Table S3, Supporting Information).

The proteins with the strongest positive and negative Spearman correlations (and adjusted p-value < 0.05) to cell density and pCO_2 are presented in a co-expression subnetwork (**Figure 4**A). A .SIF-file of the Spearman correlations is available in Supporting Information (S5).

Many proteins that showed correlation with cell density and pCO_2 were related to cellular structure and stress fiber assembly. Conceivably, this was a result of an escalation of mechanical forces in the bioreactor. For example, decorin showed a high positive correlation with the cell density. Decorin is important for organizing the supportive collagen fibrils and, among many functions, allows the extra-cellular matrix (ECM) to withstand more physical stress.[41] Cytoskeletal proteins also increased in correlation with the cell density. Spectrin, for example, is important for membrane integrity, shape, and structure.[42] The increase in α-actinin could be a sign of stress fiber assembly. These fibers can be formed when cells are exposed to mechanical forces[43] and are, for instance, important for cell-ECM adhesion and cell morphogenesis through their contractile nature.[44] The assembly of stress fibers could therefore explain the decrease in cell diameter observed at higher cell densities. The neural cell adhesion molecule is also associated with formation of stress fibers[45] and is important to maintain cellular homeostasis.[46] Aspartyl aminopeptidase has been suggested as an enzyme involved in stabilizing the actin cytoskeleton.[47] Septin-2 and adenylyl cyclase-associated protein positively correlated with pCO_2 and might also be involved in stress fiber formation.[48,49] Plasminogen activator inhibitor 1, metalloendopeptidase, procollagen C-endopeptidase enhancer 2, stromelysin-2 are participating in cleavage of ECM proteins and showed a reduced presence as the cell density and pCO_2 increased.[50–52] Additionally, among the proteins showing a significant change when comparing low to high cell densities (see Table S2, Supporting Information), many proteins with roles in cellular structure and organization showed up. For example, myosin-9 and myosin-10, which are involved in stress fiber contractility,[53] significantly increased. Vinculin, which regulates contractile stress and thereby strengthens the mechanical stability under external forces,[54] also showed a significant increase. Interestingly, the abundance of zyxin, which rapidly responds to mechanical forces and recruits α-actinin to preserve the integrity of the actin cytoskeleton,[55] was significantly lower towards the end of the experiment. Cysteine-rich protein 2, which is also associated with stress fibers and interacts with α-actinin and zyxin, showed negative correlation with pCO_2.[56] Although the cell density and pCO_2 are linked and showed a high correlation (0.72), the structural proteins appeared more closely associated to the cell density than to pCO_2. Notice as well that, as showed in Figure 1B, pCO_2 was mainly $\leq$20 kPa (i.e., 150 mm Hg), except after day 44 where it was close to 30 kPa (i.e., 225 mm Hg). Proteasome components were correlating positively with both cell density and pCO_2. The proteasome, further discussed below, has multiple functions.

3.4. Metabolomics and Proteomics Data Indicate Oxidative Stress at Very High Cell Densities

The exometabolome was highly stable in perfusion. Nevertheless, a couple of potential extracellular biomarkers varied and were identified as significant biomarkers of the cell density in TFF#10 run: Met-X-Y, methionine and pyroglutamate. The

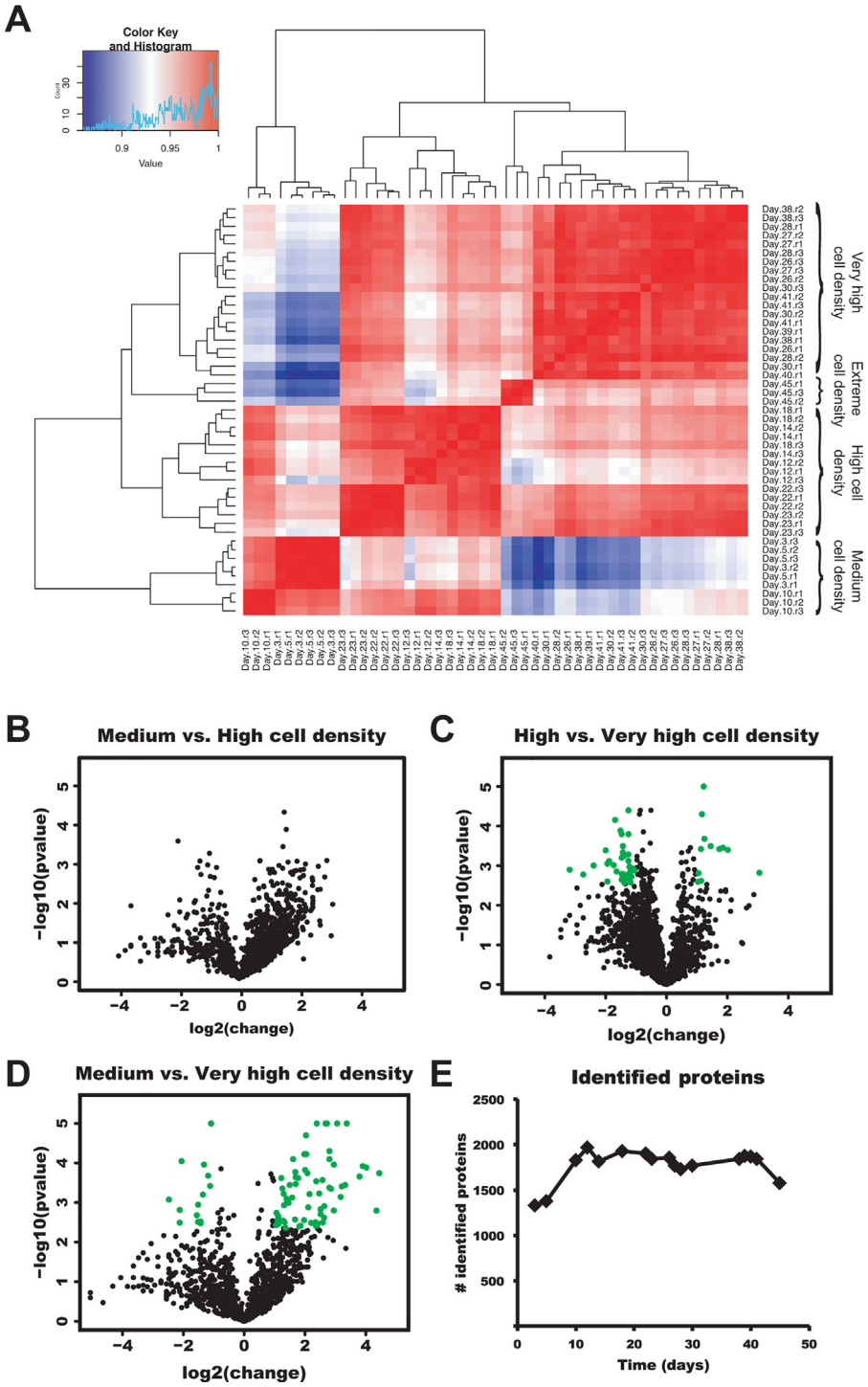

Figure 3. Sample distribution and cell density comparisons. A) Samples and replicates displayed high similarity with Pearson correlations, especially considering the exceptionally wide range of cell densities in the experiment. Most of the comparisons had a correlation coefficient above 0.9. The samples were interpreted as four main clusters: medium cell density, with samples ranging from 3 to 30 MVC mL^{-1}; high cell density, 30 to 82 MVC mL^{-1}; very high cell density, 94 to 126 MVC mL^{-1}; extreme cell density, 201 MVC mL^{-1}. The medium, high and very high groups were compared with Welch's *t*-test. A doubling or halving in abundance and adjusted *p*-values below 0.05 were considered a significant change. B) No significant changes were seen between medium and high cell densities, (C) 51 proteins (2.9% of all compared proteins) had changed between high and very high cell densities, and (D) 83 proteins (7.2%) had changed between medium and very high cell densities. E) Close to 2000 proteins were identified in each sample, except for the first two and the last sample which were closer to 1500 proteins.

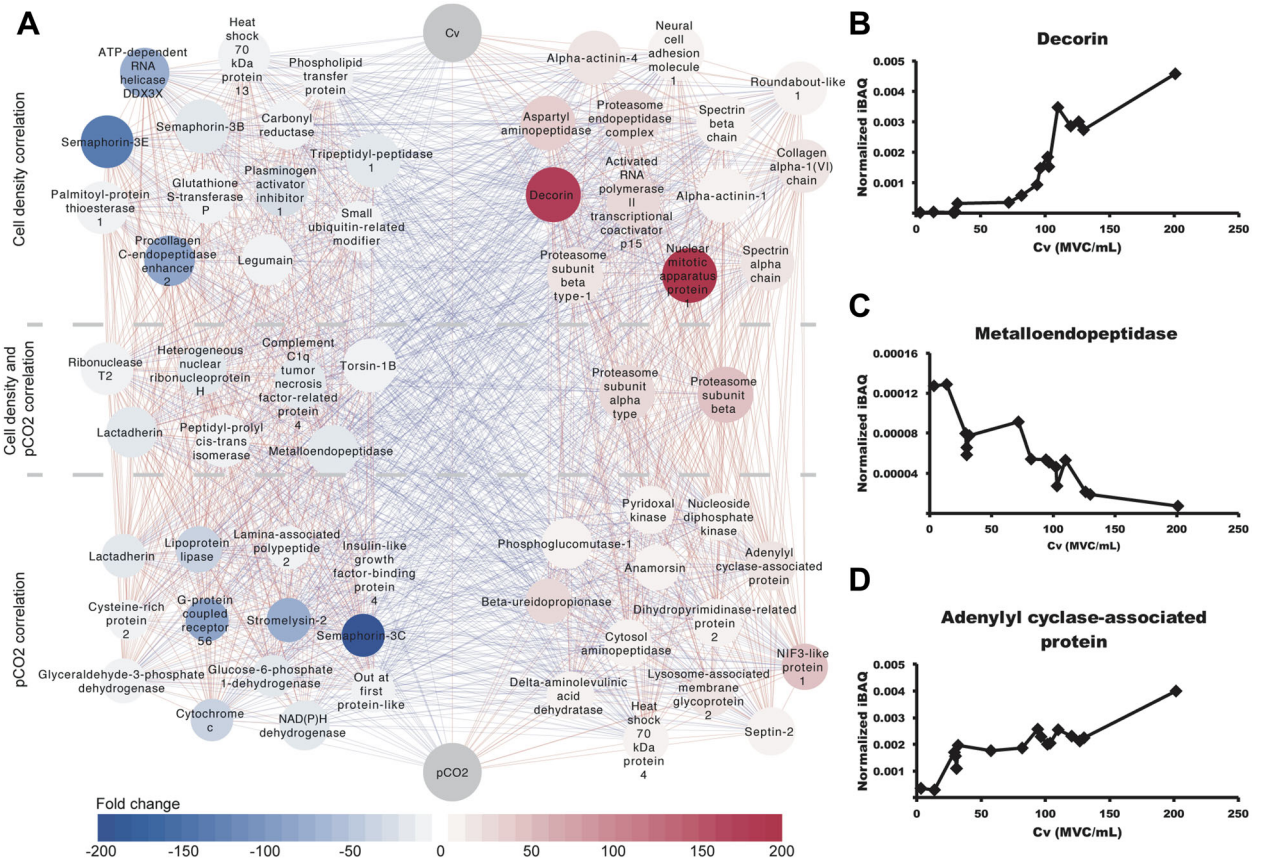

Figure 4. Correlations of the proteome with cell density and pCO_2. A) The twenty-best positive and negative spearman correlations with both cell density and pCO_2 presented in a co-expression subnetwork. In total, only 61 proteins are shown due to duplicate entries (mainly proteasome subunits) and proteins correlating with both cell density and pCO_2. The correlation coefficients for the cell density ranged from 0.91 to 0.98 (positive) and −0.84 to −0.94 (negative) and for pCO_2 from 0.78 to 0.86 (positive) and −0.70 to −0.85 (negative). The circle size corresponds to the coefficient values while the color corresponds to the fold change between the lowest and the highest iBAQ value. All the correlations had an adjusted *p*-value below 0.05. B–D) Examples of proteins with positive (decorin and adenylyl cyclase-associated protein) and negative correlation (metalloendopeptidase).

variation of these metabolites as a function of the viable cell density is shown in **Figure 5**A–C. These metabolites can be coupled to the glutathione metabolism.

Glutathione (GSH), γ-L-Glutamyl-L-cysteinylglycine, serves as reducing agent to protect the cells from oxidative stress caused by reactive oxygen species (ROS). It is a tripeptide synthesized from amino acids L-cysteine, L-glutamic acid, and glycine. Methionine (Met) is considered as a cysteine precursor through the transsulfuration (or cystathionase) pathway, which is part of the methionine catabolism that releases free cysteine for GSH synthesis.[57] The transsulfuration pathway is considered very important for cysteine supply due to its fast autoxidation to cysteine.[57,58] Hence, we postulate that the tripeptide Met-X-Y acts as a precursor for Met and that its dramatic decrease at $Cv \geq 110\ MVC\ mL^{-1}$ implies an important need of cysteine for GSH synthesis, in line with the fact that the methionine residual concentration became lower at $Cv \geq 110\ MVC\ mL^{-1}$.

Pyroglutamate (5-oxoproline) is a cyclic form of glutamate and is involved in extracellular glutamine decomposition; it is also a precursor of glutamate in γ-glutamyl cycle that continuously generates cysteine from GSH. It has been reported that glutathione synthetase (GSS) deficiency leads to low GSH levels and and high levels of pyroglutamate, probably due to enhanced γ-glutamylcysteine synthesis, since GSH was reported previously showing inhibiting feedback on glutamate-cysteine ligase (GCL).[59]

Interestingly, the enzymes responsible for de novo GSH synthesis, both GSS and GCL, soared as the cell density increased from 130 to 200 MVC mL^{-1} (Figure 5D,E). Glutathione reductase (GSR), which recycles oxidized GSH through the reduction of glutathione disulfide (GSSG), presented a similar raise towards the end of the experiment (Figure 5F). Furthermore, glutathione reductase requires NADPH to reduce glutathione disulphide (GSSG) back to GSH. To this end, isocitrate (NADP), the enzyme catalyzing the conversion of NADP+ to NADPH increased steadily throughout the run (Figure 5G). Glutathione, in co-action with either glutathione peroxidase or glutathione S-transferases, is used to protect the cells against ROS molecules. Two glutathione S-transferases displayed a drastic increase toward extreme cell densities (Figure 5H,I) while two others showed a decrease over time. Six other S-transferases presented inconclusive trends. Glutathione S-transferases have been shown to have different roles in different kinds of oxidative stress.[60] Both the glutathione S-transferases as well as glutathione peroxidase can catalyze the

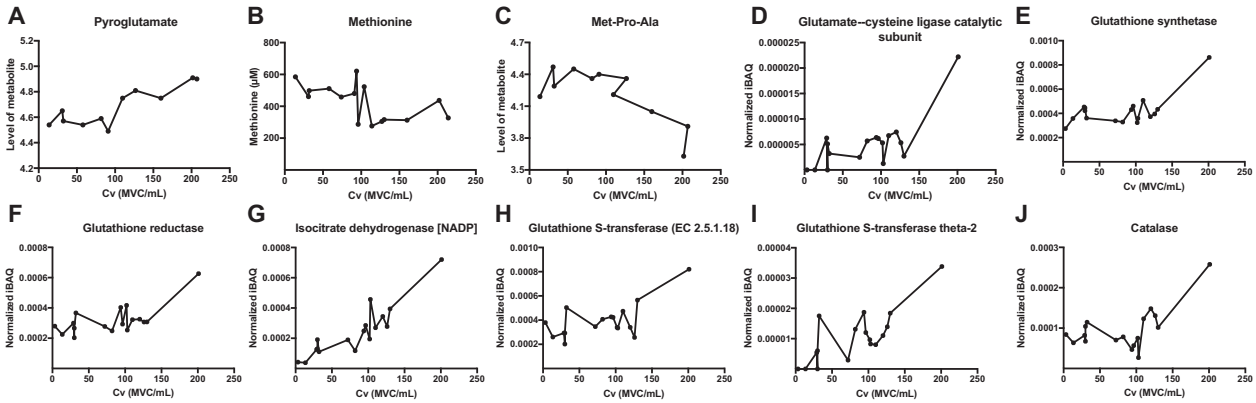

Figure 5. Examples of metabolites and proteins coupled to oxidative stress. A–C) Examples of metabolites that changed at higher cell densities. D–G) Examples of proteins involved in glutathione production increasing drastically at the highest cell density. H–J) Enzymes involved in ROS detoxification towards the highest cell densities.

conjunction of GSH to organic hydroperoxides, but glutathione peroxidase can additionally turn harmful hydrogen peroxide into oxygen and water. Although glutathione peroxidase was not observed to increase, another enzyme, catalase, which also can disassemble hydrogen peroxide[61] displayed a rapid escalation as the cell density reached above 110 MVC mL^{-1}, see Figure 5H–J. In Figure 4A, proteasome subunits correlated positively with the cell density and pCO_2. This was presumably due to an increase of misfolded or aggregated proteins as the cell density augmented, in association with the fact that oxidatively damaged proteins tend to form aggregates that the proteasome must then degrade to maintain cellular homeostasis.[62] As final remark, one can wonder if the variations observed in the molecules associated to the glutathione metabolism/ROS could be due to the cell age rather than the high cell density as both jointly increased with time in TFF#10 culture (see Figure S4K, Supporting Information). It is known that the glutathione metabolism can change with aging in the body or in primary cell cultures however this has not been reported for established cell lines unless the cells are submitted to unfavorable conditions like in fed-batch at stationary phase. To address this for TFF#10 culture, the metabolites and proteins coupled to oxidative stress (given in Figure 5) were represented as function of the number of generations (see Figure S4, Supporting Information). At high cell densities (i.e., between 110 and more than 200 MVC mL^{-1}), most of these molecules (in particular Figure S4C–S4J, Supporting Information) were influenced by the cell density but not by the generation number, which then varied only between 17.5 and 19.2. This confirmed that cell aging was not responsible for the variations in the glutathione metabolism/ROS.

4. Discussion

In order to open up the black box of bioprocess, we have analyzed how the metabolomic and proteomic landscape in a perfusion process changed over time as the cell density was increased to extremely high levels. Our main conclusion of this analysis is that the perfusion mode allows for a strikingly stable environment for the cells, both reflected in the comparison of metabolome and proteome from relatively low up to extremely high cell densities.

Apart from the general picture of a stable environment, glutathione related metabolism of CHO cells was changed at very high cell densities exceeding 110 MVC/mL, indicating a sudden raise in oxidative stress. Signs of oxidative stress were also visible in the proteomics data at higher cell densities with catalase beginning to increase at 110 MVC mL^{-1}, proteasome subunit increasing with cell density and, at 200 MVC mL^{-1}, a much higher abundance of enzymes involved in GSH production and regeneration.

Further focusing on the high cell density part of the culture, many proteins related to the cellular structure and reorganization increased in correlation with the cell density and pCO_2, showing in particular an increase in stress fiber formation. The dynamic viscosity is enhanced at higher cell densities, which results in an increase in shear stress. When exposed to shear stress, the extension of stress fibers is independent of the Zyxin/VASP complex,[63] which possibly could explain why an increase in Zyxin was not seen. Also, as the cell density increases, the distance between the cells becomes smaller (i.e., $\leq$2 um).[5] This results in a higher collision frequency between the cells and the cells are thereby exposed to more mechanical force that can promote stress fiber assembly. Stress fibers influence the cell shape and stiffness[64] and we hypothesize that the cells are muscling up to sustain increasing mechanical forces and that this could explain the decrease in cell diameter observed at higher cell densities. The cell density and pCO_2 correlated well with each other and it was therefore difficult to differentiate the results. Notice however that, except after day 44, pCO_2 varied moderately between 10 and 20 kPa. A total of 20 kPa is a level potentially encountered in large-scale fed-batch bioreactors, and can cause reductions of the cell growth and/or product productivity as well as product quality change; however, these alterations are often not too severe and therefore acceptable. As more structural proteins had a higher correlation with the cell density than with pCO_2 and the pCO_2 level was mostly $\leq$20 kPa, it is likely that these observations were due to the cell density rather than to the pCO_2.

As showed by increasing amount of produced antibodies retained by the hollow fiber filter after one culture week, a sieving effect occurred with time due to DNA and cell debris

accumulating in the bioreactor.[6] Potentially, this could introduce an artificial accumulation of large interconnected proteins in the reactor and could slightly skew the cell biology interpretation of the results. It is however noticeable that many smaller proteins also showed a dramatic increase; hence, protein increase was not only an artefact due to sieving, and the fact that decorin increased a lot more than collagen, could not be explained by the sieving effect of the filter.

The proteasome subunits increased with the cell concentration, probably due to more oxidatively damaged proteins that needed to be removed at this density. This could explain the decreased q_{MAb} and the modification of the glutamine metabolism (i.e., q_{gln} decrease) occurring at densities $\geq$130 and 160 MVC mL^{-1} respectively. q_{gln} decreased while q_{amm} remained unchanged, which is coherent with the fact that possibly more glutamine molecules became available from the protein degradation by the proteasome subunits.

Our results showed a more constant metabolic footprint for perfusion mode compared to fed-batch mode. This confirms previous results that perfusion with CSPR ensures a constant environment to the cells, which generates a constant cell metabolism.

Future studies could investigate the product quality for high-density cultivations and transcriptomics analysis could be carried out to refine our knowledge. But overall, the findings presented in this work suggest that, from a biological perspective, CHO cells were cultured in perfusion at cell densities up to 100–120 MVC mL^{-1}, without major changes in their metabolism. At this cell density, we detected no alarming signs of cellular impairment and the specific productivity remained stable. Potentially at higher cell densities, alteration could occur, which could be prevented by supplementation with anti-oxidant additives. This study confirms that high cell density perfusion culture is a viable system for biopharmaceutical manufacturing.

Abbreviations

ACD, average cell diameter; BHK, Baby hamster kidney; CHO, Chinese hamster ovary; Cv, viable cell density; ECM, extracellular matrix; GCL, glutamate-cysteine ligase; GSH, glutathione; GSS, glutathione synthetase; GSSG, glutathione disulphide; LC/MS, Liquid chromatography-mass spectrometry; mAb, monoclonal antibody; MVC, million viable cells; PCA, Principal component analysis; PLS, Partial Least Square; PLS-DA, Partial Least Squares-discriminant analysis; q_{amm}, cell-specific ammonia production; q_{glc}, cell-specific glucose consumption rate; q_{gln}, cell-specific glutamine consumption rate; q_{lac}, cell-specific lactate production; q_{Mab}, cell-specific production of antibody; ROS, reactive oxygen species.

Supporting Information

Supporting Information is available from the Wiley Online Library or from the author.

Acknowledgement

L.Z. and M.L. contributed equally to this work. Dr. Leila Zamani, Dr. Ye Zhang and Dr. Veronique Chotteau gratefully acknowledge funding from Vinnova (Sweden Innovation Agency) and KTH. Magnus Lundqvist was kindly sponsored by the Wallenberg Centre for Protein Research and MedImmune, Astra Zeneca. The authors are grateful to the Department of Oncology-Pathology and the SciLife Lab of Stockholm for instrumental LC/MS support. GE Healthcare supported the previously reported studies of Clincke et al.,[5,6] from which the experimental data used in this work were obtained. We would like to acknowledge Prof. Lukas Käll for valuable advice and discussions.

Conflict of Interest

The authors declare no financial or commercial conflict of interest.

Keywords

bioreactor, CHO cells, industrial biotechnology, metabolomics, proteomics

Received: January 12, 2018
Revised: June 3, 2018
Published online: July 13, 2018

[1] S. Mercille, M. Johnson, S. Lanthier, A. A. Kamen, B. Massie, *Biotechnol. Bioeng.* **2000**, *67*, 435.
[2] T. Ryll, G. Dutina, A. Reyes, J. Gunson, L. Krummen, T. Etcheverry, *Biotechnol. Bioeng.* **2000**, *69*, 440.
[3] Y. J. Tang, R. Ohashi, J. F. P. Hamel, *Biotechnol. Prog.* **2007**, *23*, 255.
[4] D. Voisard, F. Meuwly, P. A. Ruffieux, G. Baer, A. Kadouri, *Biotechnol. Bioeng.* **2003**, *82*, 751.
[5] M. F. Clincke, C. Molleryd, Y. Zhang, E. Lindskog, K. Walsh, V. Chotteau, *Biotechnol. Prog.* **2013**, *29*, 754.
[6] M. F. Clincke, C. Molleryd, P. K. Samani, E. Lindskog, E. Faldt, K. Walsh, V. Chotteau, *Biotechnol. Prog.* **2013**, *29*, 768.
[7] G. W. Hiller, A. D. Aeschlimann, D. S. Clark, H. W. Blanch, *Biotechnol. Bioeng.* **1991**, *38*, 733.
[8] W. M. Miller, H. W. Blanch, C. R. Wilke, *Biotechnol. Bioeng.* **2000**, *67*, 853.
[9] W. S. Ahn, M. R. Antoniewicz, *Metab. Eng.* **2013**, *15*, 34.
[10] N. Carinhas, T. M. Duarte, L. C. Barreiro, M. J. Carrondo, P. M. Alves, A. P. Teixeira, *Biotechnol. Bioeng.* **2013**, *110*, 3244.
[11] W. P. Chong, S. G. Reddy, F. N. Yusufi, D. Y. Lee, N. S. Wong, C. K. Heng, M. G. Yap, Y. S. Ho, *J. Biotechnol.* **2010**, *147*, 116.
[12] W. P. Chong, F. N. Yusufi, D. Y. Lee, S. G. Reddy, N. S. Wong, C. K. Heng, M. G. Yap, Y. S. Ho, *J. Biotechnol.* **2011**, *151*, 218.
[13] S. Dietmair, M. P. Hodson, L. E. Quek, N. E. Timmins, P. Chrysanthopoulos, S. S. Jacob, P. Gray, L. K. Nielsen, *Biotechnol. Bioeng.* **2012**, *109*, 1404.
[14] C. A. Sellick, A. S. Croxford, A. R. Maqsood, G. Stephens, H. V. Westerhoff, R. Goodacre, A. J. Dickson, *Biotechnol. Bioeng.* **2011**, *108*, 3025.
[15] C. A. Sellick, A. S. Croxford, A. R. Maqsood, G. M. Stephens, H. V. Westerhoff, R. Goodacre, A. J. Dickson, *Biotechnol. J.* **2015**, *10*, 1434.
[16] S. Selvarasu, Y. S. Ho, W. P. Chong, N. S. Wong, F. N. Yusufi, Y. Y. Lee, M. G. Yap, D. Y. Lee, *Biotechnol. Bioeng.* **2012**, *109*, 1415.
[17] Z. Sheikholeslami, M. Jolicoeur, O. Henry, *J. Biotechnol.* **2013**, *164*, 469.
[18] N. Templeton, J. Dean, P. Reddy, J. D. Young, *Biotechnol. Bioeng.* **2013**, *110*.
[19] C. Goudar, R. Biener, C. Boisart, R. Heidemann, J. Piret, A. de Graaf, K. Konstantinov, *Metab. Eng.* **2010**, *12*, 138.
[20] P. K. Chrysanthopoulos, C. T. Goudar, M. I. Klapa, *Metab. Eng.* **2010**, *12*, 212.
[21] S. I. Vernardis, C. T. Goudar, M. I. Klapa, *Metab. Eng.* **2013**, *19*, 1.

[22] S. Bajad, V. Shulaev, *Methods Mol. Biol*. **2011**, *708*, 213.
[23] W. P. K. Chong, S. H. Thng, A. P. Hiu, D. Y. Lee, E. C. Y. Chan, Y. S. Ho, *Biotechnol. Bioeng*. **2012**, *109*, 3103.
[24] H. Idborg, L. Zamani, P. O. Edlund, I. Schuppe-Koistinen, S. P. Jacobsson, *J. Chromatogr. B* **2005**, *828*, 9.
[25] H. Idborg-Bjorkman, P. O. Edlund, O. M. Kvalheim, I. Schuppe-Koistinen, S. P. Jacobsson, *Anal. Chem*. **2003**, *75*, 4784.
[26] R. Devantier, B. Scheithauer, S. G. Villas-Boas, S. Pedersen, L. Olsson, *Biotechnol. Bioeng*. **2005**, *90*, 703.
[27] M. B. Haack, A. Eliasson, L. Olsson, *J. Biotechnol*. **2004**, *114*, 199.
[28] J. E. Jackson, *A User's Guide to Principal Components*. John Wiley & Sons, Inc., **1991**.
[29] S. Wold, M. Sjostrom, L. Eriksson, *Chemometrics Intell. Lab. Syst*. **2001**, *58*, 109.
[30] G. Zhu, L. Sun, T. Albanetti, T. Linkous, C. Larkin, R. Schoner, J. B. t. McGivney, N. J. Dovichi, *Biotechnol. Bioeng*. **2016**, *113*, 2140.
[31] W. Sommeregger, P. Mayrhofer, W. Steinfellner, D. Reinhart, M. Henry, M. Clynes, P. Meleady, R. Kunert, *Biotechnol. Bioeng*. **2016**, *113*.
[32] H. Dorai, *J. Proteomics Bioinformatics* **2013**, *06*, 99.
[33] K. M. Aberg, E. Alm, R. J. O. Torgrip, *Anal. Bioanal. Chem*. **2009**, *394*, 151.
[34] K. M. Aberg, R. J. O. Torgrip, J. Kolmert, I. Schuppe-Koistinen, J. Lindberg, *J. Chromatogr.* **2008**, *1192*, 139.
[35] E. Tengstrand, J. Rosen, K. E. Hellenas, K. M. Aberg, *Anal. Bioanal. Chem*. **2013**, *405*, 1237.
[36] J. R. Wisniewski, A. Zougman, M. Mann, *J. Proteome Res*. **2009**, *8*, 5674.
[37] J. Rappsilber, M. Mann, Y. Ishihama, *Nat. Protoc*. **2007**, *2*, 1896.
[38] J. A. Vizcaino, A. Csordas, N. del-Toro, J. A. Dianes, J. Griss, I. Lavidas, G. Mayer, Y. Perez-Riverol, F. Reisinger, T. Ternent, Q. W. Xu, R. Wang, H. Hermjakob, *Nucleic Acids Res*. **2016**, *44*, D447.
[39] J. Cox, M. Mann, *Nat. Biotechnol*. **2008**, *26*, 1367.
[40] C. W. Lim, S. H. Tai, S. H. Chan, *Amb Express* **2012**, *2*, 43.
[41] Y. Nomura, *Connect. Tissue Res*. **2006**, *47*, 249.
[42] R. Zhang, C. Zhang, Q. Zhao, D. Li, *Sci. China Life Sci*. **2013**, *56*, 1076.
[43] S. Tojkander, G. Gateva, P. Lappalainen, *J. Cell Sci*. **2012**, *125*, 1855.
[44] S. Kumar, I. Z. Maxwell, A. Heisterkamp, T. R. Polte, T. P. Lele, M. Salanga, E. Mazur, D. E. Ingber, *Biophys. J*. **2006**, *90*, 3762.
[45] F. Conchonaud, S. Nicolas, M. C. Amoureux, C. Menager, D. Marguet, P. F. Lenne, G. Rougon, V. Matarazzo, *J. Biol. Chem*. **2007**, *282*, 26266.
[46] S. Jayaraman, S. Chittiboyina, Y. Bai, P. C. Abad, P. A. Vidi, C. V. Stauffacher, S. A. Lelievre, *Nucleic Acids Res*. **2017**, *45*, 11725.
[47] A. Lee, C. Slattery, D. J. Nikolic-Paterson, D. H. Hryciw, S. Wilk, E. Wilk, Y. Zhang, V. A. Valova, P. J. Robinson, D. J. Kelly, P. Poronnik, *Am. J. Physiol. Renal Physiol*. **2015**, *308*, F784.
[48] L. Dolat, J. L. Hunyara, J. R. Bowen, E. P. Karasmanis, M. Elgawly, V. E. Galkin, E. T. Spiliotis, *J. Cell Biol*. **2014**, *207*, 225.
[49] H. Zhang, P. Ghai, H. Wu, C. Wang, J. Field, G. L. Zhou, *J. Biol. Chem*. **2013**, *288*, 20966.
[50] C. F. Baicu, Y. H. Zhang, A. O. Van Laer, L. Renaud, M. R. Zile, A. D. Bradshaw, *Am. J. Physiol. Heart Circ. Physiol*. **2012**, *303*, H234.
[51] G. Cox, W. P. Steward, K. J. O'Byrne, *Thorax* **1999**, *54*, 169.
[52] O. Rechardt, O. Elomaa, M. Vaalamo, K. Paakkonen, T. Jahkola, J. Hook-Nikanne, R. M. Hembry, L. Hakkinen, J. Kere, U. Saarialho-Kere, *J. Invest. Dermatol*. **2000**, *115*, 778.
[53] T. Vallenius, *Open Biol*. **2013**, *3*, 130001.
[54] C. T. Mierke, P. Kollmannsberger, D. P. Zitterbart, J. Smith, B. Fabry, W. H. Goldmann, *Biophys. J*. **2008**, *94*, 661.
[55] M. A. Smith, E. Blankman, M. L. Gardel, L. Luettjohann, C. M. Waterman, M. C. Beckerle, *Dev. Cell* **2010**, *19*, 365.
[56] H. A. Louis, J. D. Pino, K. L. Schmeichel, P. Pomies, M. C. Beckerle, *J. Biol. Chem*. **1997**, *272*, 27484.
[57] S. C. Lu, *Biochim. Biophys. Acta* **2013**, *1830*, 3143.
[58] M. E. Anderson, *Chem. Biol. Interact*. **1998**, *111-112*, 1.
[59] Z. Z. Shi, G. M. Habib, W. J. Rhead, W. A. Gahl, X. He, S. Sazer, M. W. Lieberman, *Nat. Genet*. **1996**, *14*, 361.
[60] E. A. Veal, W. M. Toone, N. Jones, B. A. Morgan, *J. Biol. Chem*. **2002**, *277*, 35523.
[61] P. Chelikani, I. Fita, P. C. Loewen, *Cell. Mol. Life Sci*. **2004**, *61*, 192.
[62] C. T. Aiken, R. M. Kaake, X. R. Wang, L. Huang, *Mol. Cell. Proteomics* **2011**, *10*.
[63] S. Noria, F. Xu, S. McCue, M. Jones, A. I. Gotlieb, B. L. Langille, *Am. J. Pathol*. **2004**, *164*, 1211.
[64] N. Gavara, R. Chadwick, *Biomech. Model. Mechanobiol*. **2016**, *15*, 511.

